Earth and Planetary Science Letters 407 (2014) 35–47

Contents lists available at ScienceDirect

Earth and Planetary Science Letters

www.elsevier.com/locate/epsl

Provenance of the upper Miocene–Pliocene Red Clay deposits of the Chinese loess plateau

Junsheng Nie [a,b,c,*], Wenbin Peng [a], Andreas Möller [c], Yougui Song [b], Daniel F. Stockli [d], Thomas Stevens [e], Brian K. Horton [f], Shanpin Liu [a], Anna Bird [g], Jeffrey Oalmann [c], Hujun Gong [h], Xiaomin Fang [i]

[a] MOE Key Laboratory of Western China's Environmental Systems, Collaborative Innovation Centre for Arid Environments and Climate Change, Lanzhou University, Lanzhou 73000, China
[b] State Key Laboratory of Loess and Quaternary Geology, Institute of Earth Environment, Chinese Academy of Sciences, Xi'an, P.O. Box 17, 710075, China
[c] Department of Geology, University of Kansas, 1475 Jayhawk Boulevard, Lawrence, KS 66045, USA
[d] Department of Geological Sciences, Jackson School of Geosciences, University of Texas, Austin, TX 78712, USA
[e] Department of Earth Sciences, Villavägan 16, Uppsala University, 75236 Uppsala, Sweden
[f] Department of Geological Sciences and Institute for Geophysics, Jackson School of Geosciences, University of Texas, Austin, TX 78712, USA
[g] Department of Geography, Environment and Earth Sciences, University of Hull, Cottingham Road, Hull, HU6 7RX, UK
[h] State Key Lab of Continental Dynamics, Department of Geology, Northwest University, Xian 710069, China
[i] Key Laboratory of Continental Collision and Plateau Uplift, Institute of Tibetan Plateau Research, Chinese Academy of Sciences, Beijing 100085, China

ARTICLE INFO

Article history:
Received 18 February 2014
Received in revised form 11 September 2014
Accepted 15 September 2014
Available online xxxx
Editor: T.M. Harrison

Keywords:
provenance
Red Clay
loess
Pliocene
U–Pb geochronology
zircon

ABSTRACT

A clear understanding of the provenance of late Cenozoic Chinese loess and the underlying Red Clay deposits will shed light on the history and mechanisms of Asian aridification. Although much progress has been made in understanding the source of Quaternary loess on the Chinese Loess Plateau (CLP), the provenance of the underlying upper Miocene–Pliocene Red Clay sequence is largely unknown. Here we present the first provenance history of the Red Clay sequence based on zircon U–Pb ages from the central CLP. Visual and statistical analyses of the U–Pb age populations and comparison with results from potential source regions reveals that (1) the lowermost Red Clay of the late Miocene (depositional age of ~8 Ma) is likely sourced from the nearby Liupan Mountains and the Qaidam Basin; (2) the middle Red Clay (5.5–4 Ma) of the early-mid Pliocene is sourced mainly from the Taklamakan desert, transported via lower-level westerly winds; (3) the upper Red Clay of the late Pliocene (~3 Ma) is sourced from mixed areas, although western source materials from middle-northern Tibetan plateau (including Qaidam Desert sediments and materials eroded from the Qilian Mountains) sediments appear to dominate; and (4) the Quaternary loess is also sourced from mixed source regions, albeit with dominant northern CLP proximal desert sediments transported via winter monsoon winds, which in turn may be transported from mountain source regions of the northeastern Tibet and Gobi Altai via major river systems. This long term shift in sources suggests a progressive eastward aridification during the Pliocene in Asia with the specific timing of provenance shifts synchronous with large-scale climatic transitions and Tibetan uplift, demonstrating that Asian desertification is controlled by both factors.

1. Introduction

Aridification is one of the most severe environmental problems humanity has faced over the last century. It is particularly pronounced in northern China: based only on a partial compilation of data, the annual economic loss associated with aridification in northern China is estimated to be above 100 billion Renminbin (¥), equivalent to ca. 16.5 billion US$, since the 1990's (Fu and An, 2002).

More widely, the formation of the arid environment in central Asia has a complex background. Several factors, notably Cenozoic cooling, Tibetan Plateau uplift, and retreat of the Paratethys Sea, are all implicated in causing inland Asian aridification and desertification (An et al., 2001; deMenocal and Rind, 1993; Guo et al., 2002; Li, 1995; Ramstein et al., 1997; Rea et al., 1998; Ruddiman and Raymo, 1988; Zachos et al., 2001). Furthermore, Asian deserts, which lie directly upwind of the Pacific Ocean, have

* Corresponding author at: MOE Key Laboratory of Western China's Environmental Systems, Collaborative Innovation Centre for Arid Environments and Climate Change, Lanzhou University, Lanzhou 73000, China.
E-mail addresses: jnie@lzu.edu.cn, niejunsheng@gmail.com (J. Nie).

http://dx.doi.org/10.1016/j.epsl.2014.09.026
0012-821X/

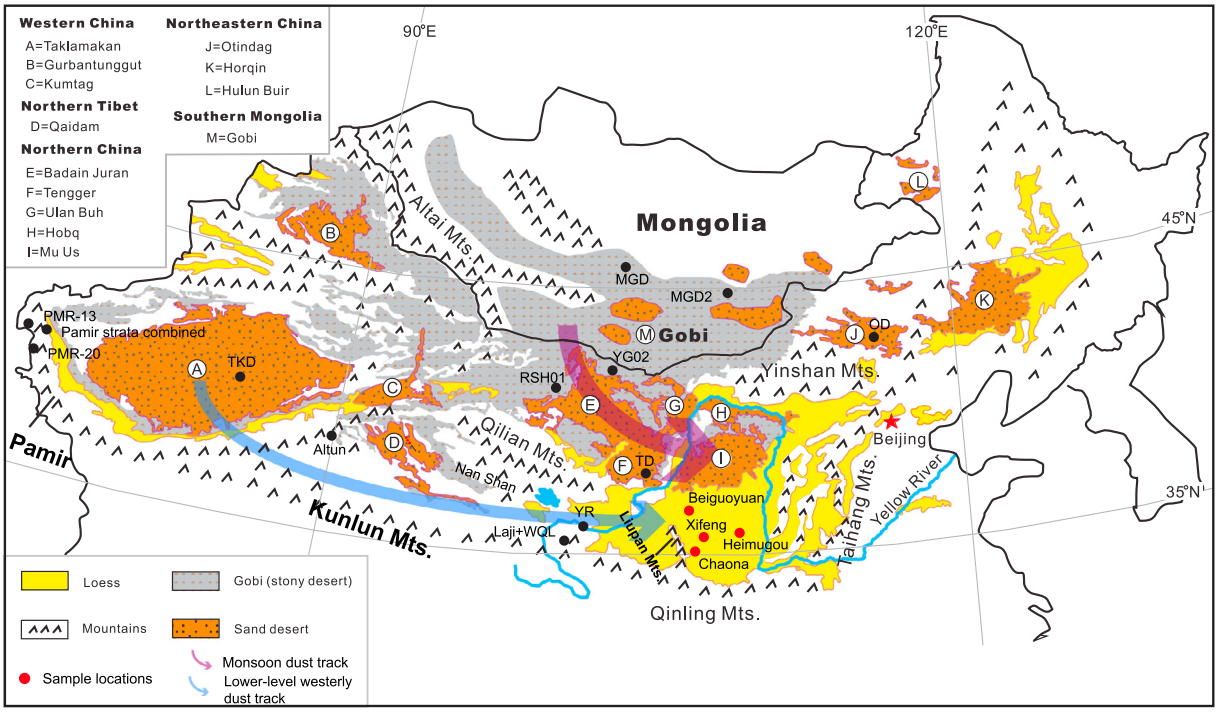

Fig. 1. Loess distribution in northern China and potential source regions and dust transport routes. Revised from Xiao et al. (2012). Approximate sample locations of loess and Red Clay samples (red dots) and source samples (black dots) are shown. Locations of samples from the Qaidam Basin (D) and the Mu Us Desert (I) are not shown due to space limitations. The dot labeled as Laji + WQL indicates the approximate location of 9 rivers draining the Laji and the West Qinling Mountians (Lease et al., 2007). (For interpretation of the references to color in this figure legend, the reader is referred to the web version of this article.)

been argued to be an active player in controlling climate changes at orbital timescales (Watson et al., 2000). Fe from dust is a limiting nutrient for ocean plankton and higher dust input during glacial periods has been argued to amplify glacial climate cooling by cycling more carbon from the atmosphere to the deep ocean (Watson et al., 2000). Thus, research about Asian aridification is of interest both scientifically and economically.

Preventing contemporary aridification relies on a detailed understanding of its past development to identify the primary causal mechanisms. However, the aridification history in central Asia is largely unknown, mainly because paleoclimate records from inland Asia are sparse and incomplete, making a coherent reconstruction of inland Asian aridification history difficult. For example, paleomagnetic dating of eolian sediments suggests that formation of the Taklamakan desert in the Tarim basin occurred at 5.3 Ma (Sun and Liu, 2006), whereas the oldest eolian sediments in the Gurbantunggut desert of the Junggar Basin were deposited at ~24 Ma (Sun et al., 2010) (Fig. 1). In the Qaidam Basin (Fig. 1), Pliocene acceleration of aridification has been recognized based on many paleoenvironmental proxy data, including thick-bone fish fossils (Chang et al., 2008), sporopollen records (Wu et al., 2011), stable isotope data (Heermance et al., 2013), and evaporate mineral records (Li et al., 2013a), but when the aridification was initiated in the basin is less clear (Miao et al., 2012). In contrast to these results, direct drilling of the Tengger desert found that dominant eolian facies exist only since ~1.2 Ma (Li et al., 2013b), much younger than outcrop results in the other inland Asian basins. Aridification in parts of Asia may also have a much longer history, with Cretaceous eolianite sandstone sediments of desert facies underlying large parts of the Mu Us desert and Chinese Loess Plateau (CLP) (Li et al., 1999) (Fig. 1).

Different lines of evidence suggest that Asian deserts are important dust source regions for the CLP (Chen et al., 2007; Sun, 2002; Sun et al., 2001, 2008), although the role of deserts in dust production is controversial, with some authors arguing that processes operating in these regions are not conducive for producing suitable volumes of dust (Lu et al., 2011; Smalley et al., 2005). Despite this, many previous studies have focused on inferring the aridification history of inland Asia based on studying eolian sediments on the CLP (An, 2000; Ding et al., 1999; Fang et al., 1999; Lu and An, 1998; Sun et al., 1997). Two late Cenozoic eolian depositional sequences are well known from the central CLP: the Quaternary loess-paleosol sequence (~2.7–0 Ma) (Liu, 1985) and the late Miocene–Pliocene Red Clay sequence (~8–2.7 Ma) (Ding et al., 1999; Song et al., 2001; Sun et al., 1997). The Quaternary loess-paleosol sequence is the most well-studied and understood sequence. Despite this, and while at present there is a consensus that this sequence is eolian, the exact provenance of this sequence is the subject of considerable recent debate (Chen et al., 2007; Chen and Li, 2013; Derbyshire et al., 1998; Guan et al., 2008; Maher et al., 2009; Nie et al., 2013; Pullen et al., 2011; Stevens et al., 2013a, 2013b, 2010; Sun et al., 2008; Xiao et al., 2012). By contrast, in addition to a lack of consensus on sources, no consensus exists as to whether the bottom part of the Red Clay sequence is eolian or water-lain (Ding et al., 1998; Guo et al., 2001; Lu et al., 2001; Miao et al., 2004). Studies arguing for a water-lain environment propose that the lower part of the Red Clay sequence is probably sourced from the nearby Liupan Mountains (Guo et al., 2001). For the upper Red Clay, while there is a consensus that the sediments are eolian, opinions differ as to whether the provenance of the material is western deserts via lower-level westerly winds or northern deserts via winter monsoon winds (Ding et al., 2000; Miao et al., 2004). This severely limits the use of these deposits to shed light on the causes, extent and timing of long term Asian aridification. Note here that we use the term 'westerly' wind in the literal sense; to mean wind directed west to east, rather than only upper atmospheric level winds associated with the jet stream at the tropopause. The latter are only one facet of westerly circulation and where needed we have distinguished which we refer to.

The main reason for the debate over Red Clay source is a lack of detailed provenance work undertaken on the Red Clay sequences that can resolve multiple individual sources. To overcome this, here we investigate the provenance of the CLP Red Clay using zircon U–Pb geochronology for the first time. Zircon U–Pb ages are particularly useful in tracing sediment provenance because this technique obtains a range of U–Pb ages from many measured detrital zircon grains and thus has the potential to fingerprint multiple sources (Chang et al., 2006; Nie et al., 2010; Pullen et al., 2011; Riggs et al., 1996; Stevens et al., 2010). Although other techniques such as whole-rock Nd isotope ratios and rock magnetic analyses are useful in sourcing sediment (Chen et al., 2007; Gallet et al., 1996; Maher et al., 2009; Sun et al., 2008), they tend to integrate multiple provenance signatures, making explicit recognition of source regions difficult, especially when there are multiple potential sources. The zircon U–Pb technique has been even more widely applied since very rapid analyses by laser ablation inductively coupled mass spectrometry (LA-ICP-MS) has become routine in the study of provenance of sedimentary basins (Dickinson and Gehrels, 2008). These new data have provoked considerable debate over the provenance of the Quaternary loess-paleosol sequence since the initial use of the technique on the CLP (Stevens et al., 2010). For example, a recent combined heavy mineral and zircon U–Pb and fission-track study suggests that fluvial transport of dust from source regions on the NE Tibetan plateau is significant in loess accumulation, with dust being deflated from channels and floodplains draining the plateau before final eolian deposition, a factor that has previously been underemphasized (Stevens et al., 2013b). Furthermore, Pullen et al. (2011) compared zircon U–Pb ages between a Quaternary loess-paleosol sequence on the CLP and Plio-Pleistocene lacustrine sediments of the Qaidam Basin, and proposed that the latter is an important source for dust to the CLP. They further predicted that the dust forming loess and paleosol units should have different sources due to a hypothesized shift of the westerly winds: during glacial periods, dust sources would have been the Qaidam Basin and northern Tibetan Plateau; during interglacial periods, dust sources would be hypothesized to be northern China and southern Mongolia (Kapp et al., 2011; Pullen et al., 2011). This suggestion was tested by Xiao et al. (2012), who used zircon U–Pb dates on samples across the CLP to suggest that source regions not only shift between glacial and interglacial, but also across the CLP. However, based on large zircon datasets for the last glacial L1 loess and last interglacial S1 paleosol at Xifeng and comparisons with source regions, Che and Li (2013) concluded that the ultimate provenance of the L1 and S1 sediments on the CLP is a mix of two areas: the northern Tibetan Plateau and the Gobi Altai Mountains, with sediments mixing in the Alxa arid lands. Their study also suggests that provenance is uniform across the CLP and that no provenance shift occurred over glacial and interglacial times, a conclusion consistent with recent heavy mineral results (Nie and Peng, 2014; Nie et al., 2013).

However, no zircon U–Pb data exist for the Red Clay sequence despite the progress made using the technique on Quaternary loess and the ongoing Red Clay source debates mentioned above. Initiation of widespread eolian sedimentation on the central CLP during the Miocene–Pliocene is likely genetically related to the development and expansion of Asian dust sources, which in turn may be tied to the initiation of central Asian aridification. As such, an understanding of Red Clay sources and their depositional nature results in pinpointing of the precise timing and location of inland Asian aridification and its potential relationships to Tibetan uplift and land–sea distribution.

The debate about whether the entire or part of the Red Clay sequence is eolian or water-lain has been ongoing since the 1920's (Andersson, 1923). Andersson (1923) refers to the Red Clay sequence as the *Hipparion sp.* red soil and argues that this sequence originated as alluvial flood deposits or by oxidation of lacustrine sediments. Liu et al. (1988) presented the first magnetic fabric evidence suggesting an eolian origin for the upper part of the Red Clay sequence, which has since been supported by further magnetic studies (Liu et al., 2003; Nie et al., 2007, 2008a), grain size (Ding et al., 1998; Lu et al., 2001), and geochemical evidence (Ding et al., 2001). These studies also suggest that the bottom and middle Red Clay are also eolian. However, based on detailed soil microstructure observations, geochemical evidence, and grain size data, Guo et al. (2001) proposed that the lower Xifeng Red Clay sequence (older than ~6 Ma) is largely water-reworked sediment resulting from alluvial or slope processes, with possible minor eolian contributions. The portion between ~6 and ~3.6 Ma is interpreted as largely eolian, but significantly affected by groundwater oscillations (Guo et al., 2001). Unfortunately, Guo et al. (2001)'s work was only performed on one section, so it remains to be seen whether similar conclusions can be reached for lower Red Clay sediments of similar ages at different locations of the CLP. In addition to constraining the source regions of eolian sediments, single grain detrital zircon U–Pb dating can be used to test whether localized alluvial or more CLP distal eolian sediments dominate in the Red Clay. To address both questions we here present zircon U–Pb dating results for the well-known Chaona section (Nie et al., 2007) from the central CLP (Fig. 1) and discuss their implications for inland Asian dust source activity and its causes, as well as addressing whether the lower Red Clay at Chaona genuinely represents the late Miocene onset of eolian sedimentation at the site.

Although 500–400 and 300–200 Ma zircon U–Pb ages are prevalent in granitic rocks and Mesozoic–Cenozoic sediments both in the central Asian orogenic belt and northern Tibet, including the Songpan–Ganzi flysch (Weislogel et al., 2006; Yin and Harrison, 2000), a compilation of published zircon U–Pb data from potential source regions reveals that northern deserts generally have a stronger 300–200 Ma component, whereas the western deserts (Qaidam and Takalamakan) have more prominent 500–400 Ma components (Fig. 2 and Supplementary Fig. 1). The zircon U–Pb age distribution patterns from rivers draining northern Tibet also confirms that this area exhibits a more prominent 500–400 Ma age component than the 300–200 Ma component (Che and Li, 2013; Stevens et al., 2013b). The sediments (including fluvio-lacustrine, desert, and dry river beds) in these regions are located in the upwind direction of the CLP and as such we hypothesize that they are likely to be primary source regions for the CLP. Thus, single grain detrital zircon U–Pb dating has great potential to unravel the relationship between Red Clay accumulation and the development of Asian deserts.

2. Materials and methods

Red Clay samples were taken at ~190, ~215, ~245 and ~300 m depth of the Chaona section from the central CLP, corresponding to ~3, ~4, ~5.5 and ~8 Ma depositional ages, respectively, based on magnetostratigraphic dating (Song et al., 2001). In addition, in order to test the hypothesis that the base of the Red Clay is sourced from the Liupan Mountains, seven samples were taken from Cretaceous strata of the Liupan Mountain for comparison; for each Liupan Mountain sample, we randomly measured 20 zircon grains yielding a combined total of 140 (hereafter referred to as Liupan). We decided to use the combined data instead of data from one stratigraphic level as we anticipate that a river flowing from the upper part of the Liupan Mountains bringing materials to the Chaona section would rework older fluvial material and mix zircons from different stratigraphic levels. Furthermore, the characteristics of the drainage area of Liupan would not change significantly over this period, leading to similar age signatures.

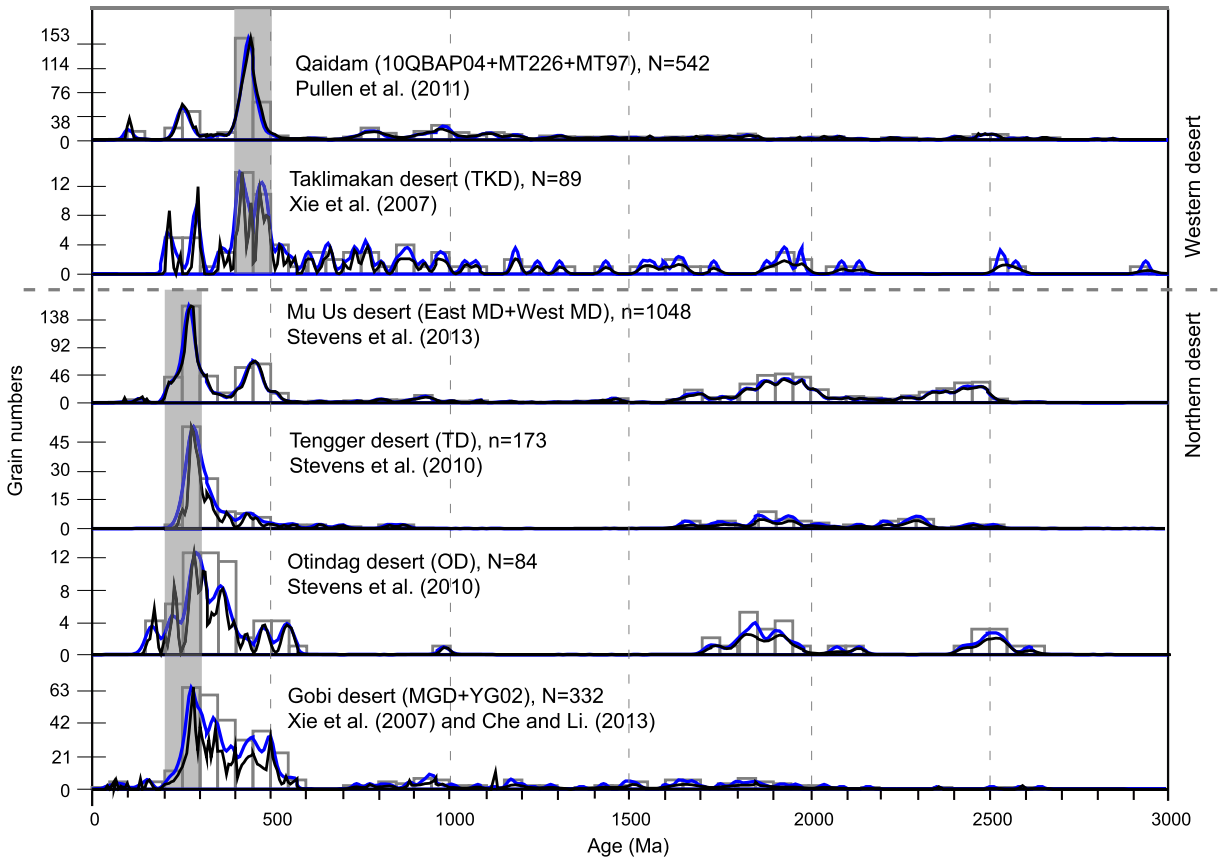

Fig. 2. A comparison of detrital zircon U–Pb ages from western and northern deserts relative to the CLP. The shaded bars highlight the most dominant zircon U–Pb age ranges. Black and blue lines are normalized probability density function (PDF) and Kernel Density Estimation (KDE) plots, respectively, and the open rectangles are age histograms. (For interpretation of the references to color in this figure legend, the reader is referred to the web version of this article.)

Detrital zircon grains were separated by standard heavy liquid techniques and selected for analysis randomly. Zircons were imaged using cathodoluminescence with a scanning electron microscope in order to characterize their internal structures. U–Pb zircon ages of the Red Clay and the Liupan Mountain samples were determined by LA-ICP-MS at the Department of Geology, University of Kansas. A Photon Machines 193 nm ArF excimer laser was used to ablate 32 μm (first-round CN-8 Ma and Liupan) and 26 μm (CN-3 Ma and CN-4 Ma) and 20 μm (CN-5.5 Ma and second-round CN-8 Ma) circular spots on zircon grains mounted in epoxy and polished to approximately half width (Supplementary Table 1). The laser was set to 3.5 $\mathrm{J\,cm^{-2}}$ fluency at a 10 Hz repetition rate with the ablated material carried to the ICP-MS in He gas with a flow rate of 0.65 $\mathrm{l\,min^{-1}}$, tied in with Ar gas at 1.2 $\mathrm{l\,min^{-1}}$ flow rate with a Y-connector 15 cm down flow from the ablation cell. Elemental fractionation, down-hole fractionation and calibration drift were corrected by bracketing measurements of unknowns with GJ1 zircon reference material (Jackson et al., 2004) and data reduction using the IOLITE software package (Paton et al., 2011). Within run reproducibility of the GJ1 reference material was better than 2% on a U–Pb age. The accuracy of the determined age was determined by repeat measurements of the Plešovice zircon reference material (Sláma et al., 2008).

The ages were rejected if discordance exceeded 10%, a practice also used by Stevens et al. (2010, 2013b), making comparison between studies simpler. $^{206}U/^{238}Pb$ ages and $^{207}Pb/^{206}Pb$ ages were used for ages younger and older than 1 Ga, respectively, although this threshold was shifted slightly for some samples to avoid splitting age clusters (Supplementary Table 1).

In order to constrain potential source areas of the Red Clay and the Quaternary loess, we compare our new results with published zircon U–Pb results from the Quaternary loess and paleosol on the CLP and from potential source areas (Table 1). Since the available dataset is large, we use the newly developed non-matrix multidimensional scaling (MDS) statistical technique to help view the data (Vermeesch, 2013). The non-metric MDS technique is based on the K–S statistical method and works in a similar way to principal component analysis, which is widely used in heavy mineral analysis. There are some limitations inherent to this technique, such as the method being more sensitive to the strongest mode and not sensitive to tail areas of the data distribution, and it does not take into account the precision of the data. However, in spite of these limitations, MDS provides a visually effective, quantitative way for comparing zircon U–Pb data and has been shown to effectively differentiate between sediment with different source characteristics (Stevens et al., 2013b). This is difficult to do by the human eye with multiple age density diagrams when the datasets are very large, making this visualization technique critical to interpret such large datasets. We also show the zircon U–Pb data in probability density functions (PDF) (Ludwig, 2003), Kernel Density Estimators (KDE) (Vermeesch, 2012), and histogram diagrams for visual comparison. However, we emphasize that we do not draw conclusions about provenance based exclusively on similarity or neighboring relationship in the MDS, KDE or PDF plot because of the likelihood of sediment mixing from multiple sources. Nearest neighbors in MDS plots can be used to consider likely possible sources but are used in tandem with KDE and PDF plots and available geological evidence in the potential source regions to consider the potential input of sediment from multiple sources.

Table 1
Zircon U–Pb samples from potential source regions.

Sample ID	Description	Refrence
Altun	Igneous	Gehrels et al. (2003)
East MD	Surface sand samples from the East Mu Us desert	Stevens et al. (2013a, 2013b)
YG02	One fluvial sample draining the south frank of the Gobi Altay Mts.	Che and Li (2013)
MGD	Surface sand samples from the northern Monglian Gobi desert	Xie et al. (2007)
Nanshan	Igneous samples from Nanshan	Gehrels et al. (2003)
OD	Surface sand samples from the Otindag desert	Stevens et al. (2010)
Pamir strata combined	Jurassic–Miocene detrital samples from Oytag, Pamir's northeastern margin	Bershaw et al. (2012)
Qilian	Igneous ages from the Qilian Shan	Gehrels et al. (2003)
10QBAP04	Qaidam Quaternary alluvium	Pullen et al. (2011)
MT226	Qaidam Pio-Quaternary lucstrine	Pullen et al. (2011)
MT97	Qaidam Pio-Quaternary lucstrine	Pullen et al. (2011)
RSH01	One fluvial fan sample draining the north frank of the Qilian Mts., with possibly eolian input of materials from the Gobi Altai Mts.	Che and Li (2013)
TKD	Surface sand sample from the East Taklimakan desert	Xie et al. (2007)
TD	Surface sand samples from the Tengger desert	Stevens et al. (2010)
West Qinling	River sand samples draining the west Qinling Mts.	Lease et al. (2007)
PMR-13	Meta-sedimentary rock from Muji Valley, the West Kunlun terrane	Bershaw et al. (2012)
PMR-20	Meta-sedimentary rock from Muji Valley, the West Kunlun terrane	Bershaw et al. (2012)
West MD	Surface sand samples from the West Mu Us desert	Stevens et al. (2013a, 2013b)
YR	One modern Yellow river sand sample from ~100 km upstrem from Lanzhou	Stevens et al. (2013a, 2013b)

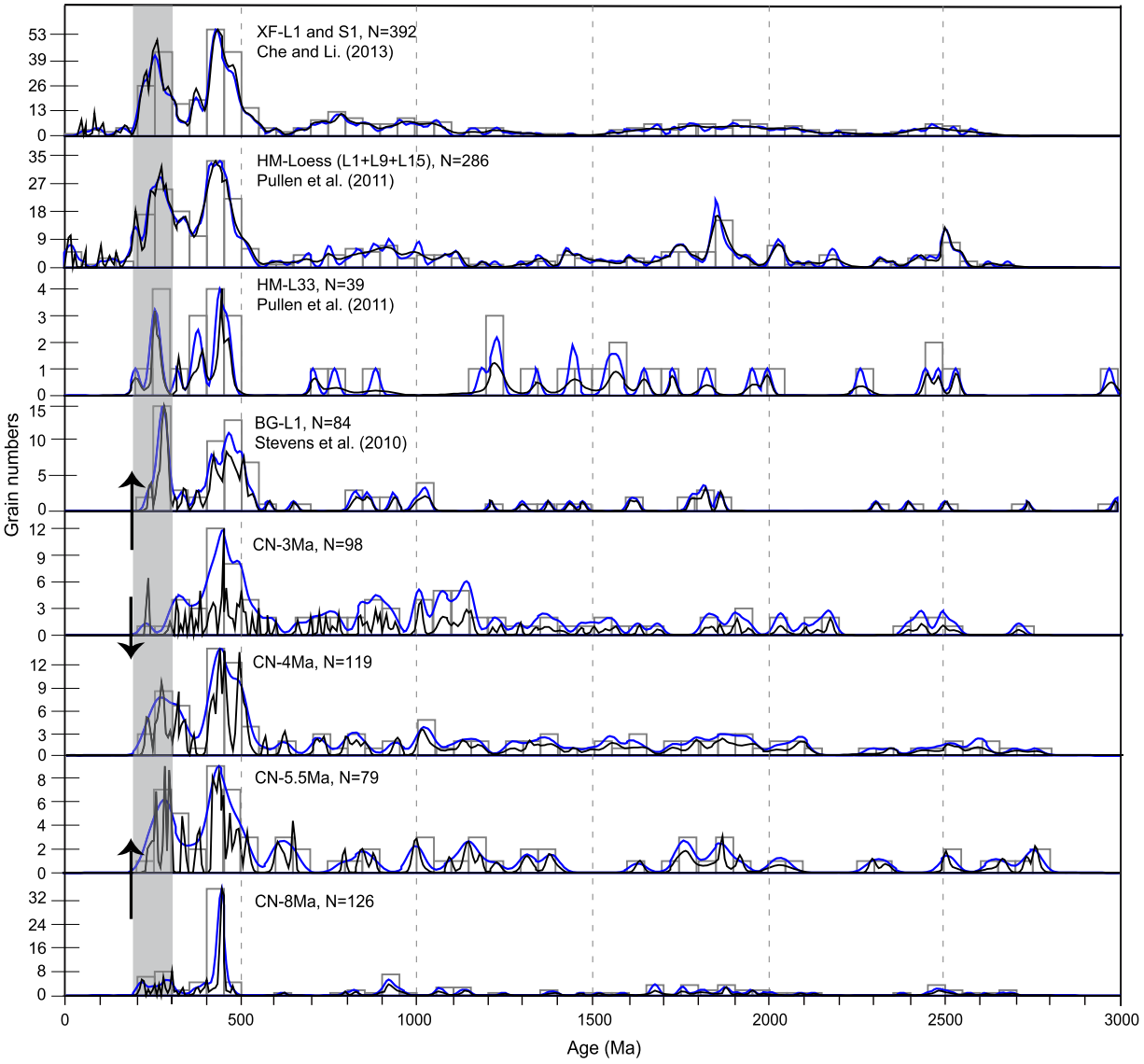

Fig. 3. A comparison of detrital zircon U–Pb ages between Quaternary loess and paleosol samples and the Miocene–Pliocene Red Clay samples. The Red Clay samples are from the Chaona section. Black and blue lines are normalized probability density function (PDF) and Kernel Density Estimation (KDE) plots, respectively, and the open rectangles are age histograms. The shaded bar marks age range 300–200 Ma and the upward and downward arrows indicate upsection increase and decrease of the 300–200 Ma age population, respectively. (For interpretation of the references to color in this figure legend, the reader is referred to the web version of this article.)

3. Results

Fig. 3 allows a comparison of zircon U–Pb ages from the ~8, ~5.5, ~4, ~3 Ma Red Clay samples from Chaona on the central CLP (hereafter CN-8 Ma, CN-5.5 Ma, CN-4 Ma, CN-3 Ma, respectively) with the last glacial loess sample (L1) from Beiguoyuan (hereafter BG-L1), Huanxian County, on the northern CLP (Stevens et al., 2010), the last glacial L1 loess and the last interglacial S1 paleosol from Xifeng (hereafter XF-L1 and XF-S1, respectively) (Che and Li, 2013) and the Quaternary loess samples (L33, L15, L9 and L1) from Heimugou (hereafter HM-L33, HM-L15, HM-L9 and HM-L1), Luochuan County, on the central CLP (Pullen et al., 2011) (Fig. 1; for a more detailed comparison, please see Supplementary Fig. 2). Note that all samples and abbreviations are listed in Table 1. It is clear from Fig. 3 that both the Red Clay and loess-paleosol samples have most ages distributed between 600–200 Ma with elevated age peaks at 500–400 Ma and 300–200 Ma. For ages older than 600 Ma, it is difficult to compare the visual characteristics of the data distribution between these samples (Fig. 3).

For the Red Clay sequence, the relative proportion of the 300–200 Ma ages changes twice: it increases from being nearly absent at the bottom (CN-8 Ma) to the middle Red Clay (CN-5.5 Ma and CN-4 Ma) and then decreases again from the middle to the upper Red Clay (CN-3 Ma) (Fig. 3). We note that using a 30% discordance filter does not change this up-section trend (Supplementary Fig. 3).

The age distribution of CN-8 Ma is markedly different from CN-3 Ma (Fig. 3 and Supplementary Fig. 4). CN-8 Ma has 32% zircons with ages between 450 and 400 Ma, whereas CN-3 Ma only has 12%, similar to the proportions shown in CN-5.5 Ma and CN-4 Ma, as well as the Quaternary samples, which have 7–17% of ages falling within the time interval 450–400 Ma (Fig. 3). A common feature of the Quaternary loess-paleosol samples is that they have a more pronounced 300–200 Ma age population than the underlying Red Clay sequence (Fig. 3 and Supplementary Fig. 2).

In non-metric MDS plots of zircon U–Pb data (stress value = 3.7%), most Quaternary loess-paleosol samples lie on the left side of the plot with the exception of HM-L33, and most Red Clay samples lie on the right side with the exception of CN-8 Ma (Fig. 4 and Supplementary Fig. 5). Because HM-L33 has too few ages (only 39) to guarantee meaningful statistical comparison with the rest of the samples, we do not discuss this sample further in the statistical analysis. CN-8 Ma and CN-3 Ma are far apart on the MDS plot and they are far apart from the two middle Red Clay samples (CN-5.5 Ma and CN-4 Ma), consistent with visual observations (Figs. 3 and 4).

To constrain the sources of the Red Clay, in a non-metric MDS plot in Fig. 5 (and Supplementary Fig. 6) we also include published zircon U–Pb data from potential source areas, including surface sediments from the modern Taklimakan desert (TKD) and Mongolian Gobi desert (MGD) (Xie et al., 2007), East and West Mu Us desert (East MD and West MD), Otindag desert (OD) and Tengger desert (TD), (Stevens et al., 2010, 2013b), a riverbed sample from the Ruoshui River draining the Qilian Mountains (RSH01) and a sample of fluvial sediment (YG02) from the south flank of the Gobi Altai Mountains (Che and Li, 2013), a modern Yellow River sediment sample (YR) (Stevens et al., 2013b), samples of modern rivers draining the Laji and the West Qinling Mountains (Laji + WQL) (Lease et al., 2007), Quaternary (10QBAP04) and Plio-Quaternary sediments (MT-97 and MT226) from the Qaidam Basin (Pullen et al., 2011), meta-sedimentary rocks from the West Kunlun terrane (PMR-13 and PMR-20), as well as detrital samples from the Jurassic through Miocene stratigraphic section in Pamir (PMR combined) (Bershaw et al., 2012), Altun, Qilian and Nanshan Mountains (Gehrels et al., 2011, 2003) (abbreviations noted in Table 1). The plot (stress value = ~9%) shows that Miocene sample

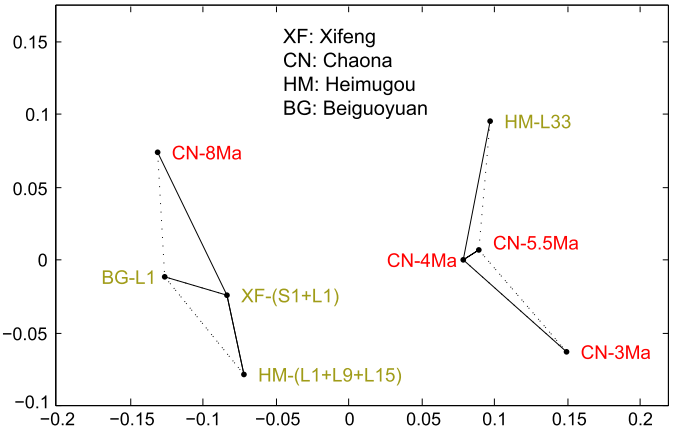

Fig. 4. Non-metric multi-dimensional scaling (MDS) plots of the Chinese loess and Red Clay U–Pb dataset. Solid lines mark the closest neighbors and dashed lines the second closest neighbors.

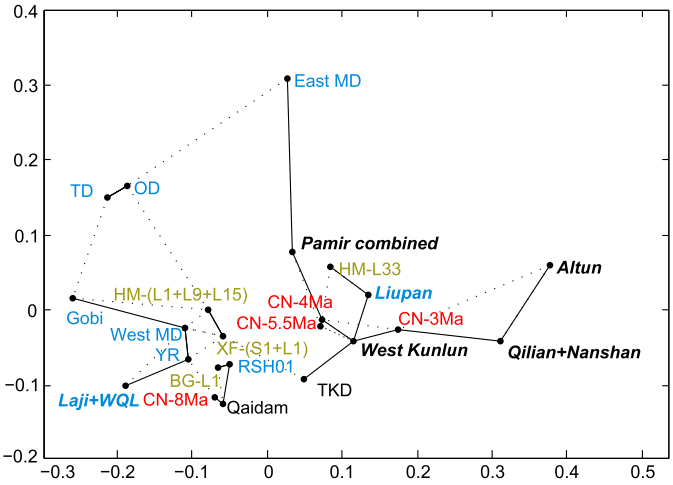

Fig. 5. Non-metric multi-dimensional scaling (MDS) plots of the Chinese loess and Red Clay U–Pb dataset and comparison with potential source regions (see text for references). Solid lines mark the closest neighbors and dashed lines the second closest neighbors. CLP proximal sources are in blue and distal sources are in black. Plio-Quaternary sources are in regular font and pre-Pliocene bedrock sources are in bold italic. Red Clay samples are in red and loess samples are in yellow. Gobi = YG02 + MGD. West Kunlun = PMR13 + PMR20. (For interpretation of the references to color in this figure legend, the reader is referred to the web version of this article.)

CN-8 Ma is close to the Qaidam samples, the two middle Pliocene Red Clay samples (CN-5.5 Ma and CN-4 Ma) are closer to the western Kunlun terrain and Pamir samples, the upper Pliocene Red Clay sample (CN-3 Ma) is closer to the western Kunlun terrain samples and Qilian and Nanshan Mountains, whereas the Quaternary loess/paleosol samples are close to TKD, West MD, RSH01, YR, TD, OD, Qaidam, and Gobi (Fig. 5 and Supplementary Fig. 6). It does not appear likely that the eastern Mu Us desert can be the major provenance source for any of the studied loess or Red Clay samples (Fig. 5).

Based on the grouping relationships expressed in Fig. 5 and Supplementary Fig. 6, we here compare zircon U–Pb data of the Mio-Pliocene Red Clay and Quaternary loess with the potential source regions. It is clear that CN-8 Ma is also similar to Qaidam samples visually (Fig. 6), consistent with the MDS plot. In addition, the Liupan sample also has a large proportion of ages falling between 450 and 400 Ma, similar to CN-8 Ma (Fig. 6). However, the Liupan sample and samples sourced from the Liupan Mountains consistently have a peak age of 430 Ma (Wang et al., 2012), whereas the CN-8 Ma and MT266 and MT-97 from Qaidam all have

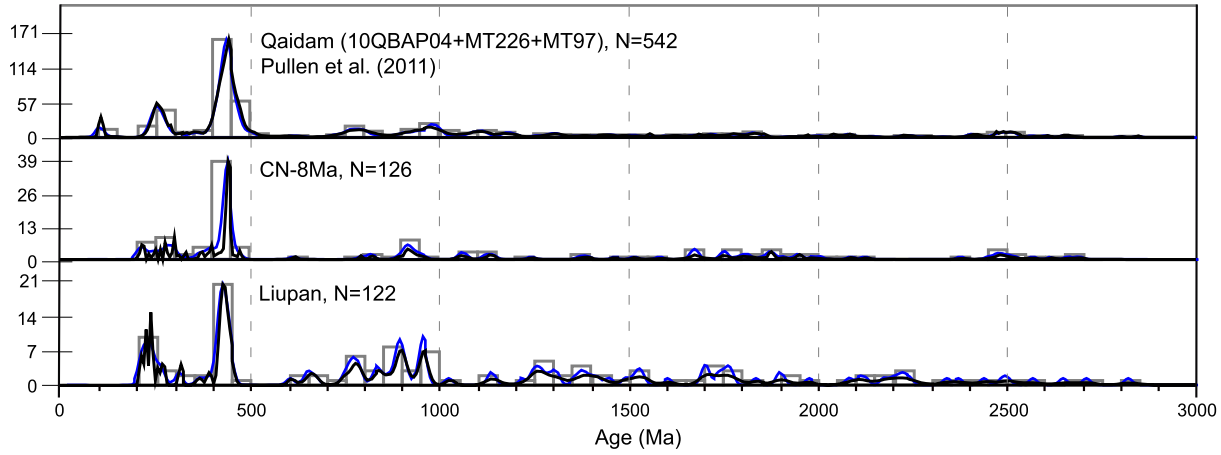

Fig. 6. A comparison of detrital zircon U–Pb ages between of CN-8 Ma, Qaidam lacustrine sediments (MT226 and MT-97), and Liupan. Black and blue lines are normalized probability density function (PDF) and Kernel Density Estimation (KDE) plots, respectively, and the open rectangles are age histograms. (For interpretation of the references to color in this figure legend, the reader is referred to the web version of this article.)

a peak age of 440 Ma (Fig. 6 and Supplementary Fig. 7). Furthermore, the Liupan sample also has more ages that fall between 300 and 200 Ma and between 1000 and 700 Ma, which makes this sample far from CN-8 Ma and closer to the other Red Clay samples on the MDS plot.

Fig. 7 and Supplementary Fig. 8 show a comparison of CN-5.5 Ma, CN-4 Ma, and CN-3 Ma with the western Kunlun terrane, TKD, Qaidam samples, and igneous zircon U–Pb data from the Qilian, Nanshan, and Altun Mountains. Consistent with the MDS plot, CN-5.5 Ma and CN-4 Ma are similar to the western Kunlun terrane samples, both having lower 300–200 Ma age population than the 500–400 Ma age population (Fig. 7 and Supplementary Fig. 8). In addition, visual comparison reveals that CN-5.5 Ma and CN-4 Ma are also similar to the TKD sample.

There is no single source that has a similar age distribution pattern similar to CN-3 Ma (Supplementary Fig. 8). However, a mixture of west Kunlun samples PMR-13 together with the Qilian and Nanshan samples is able to produce a diminished 300–200 Ma component while maintaining a strong 500–400 Ma age component (Fig. 7 and Supplementary Fig. 8). In addition, Qaidam samples also have subdued 300–200 Ma component in comparison with the 500–400 Ma component, and thus mixing the Qaidam Basin samples with the west Kunlun samples are able to produce an age distribution pattern similar to CN-3 Ma (Fig. 7 and Supplementary Fig. 8).

The Quaternary loess samples all have a more prominent component at 300–200 Ma (Fig. 8 and Supplementary Fig. 9), a feature inherent to all studied CLP proximal deserts, including the MD, the TD, the OD, and the Gobi desert, rivers draining the West Qinling, and the two rivers that drain the northeastern Tibetan plateau (the YR and the RSH) (Fig. 2). In terms of similarity to a single source, the Quaternary samples are most comparable to the West MD, the YR, and the RSH01. However, a mixture of northern desert and western desert contributions could also produce a similar age distribution pattern if the emphasis was more on northern deserts, with a more enlarged 300–200 Ma component than the Red Clay sequence. The Gobi Altai sample also shows a similar mix of components to the loess samples (Supplementary Fig. 9).

4. Discussion

Both the visual U–Pb data comparison and the quantitative MDS analysis reveal that CN-8 Ma has similar zircon U–Pb age distribution pattern to northeastern Qaidam Plio-Quaternary lacustrine samples MT226 and MT-97 (Figs. 5 and 6). Sediments from three depositional environments in the Qaidam Basin can potentially serve as provenance for the CLP. First, lacustrine sediments exposed during low lake levels can potentially contribute dusts to the CLP (Kapp et al., 2011; Pullen et al., 2011). Fang et al. (2007) reveal that northeastern Qaidam is dominated by lacustrine sediments covering the period 10–6 Ma, with the lake area possibly shrinking around 8–6.5 Ma, as is indicated by increased sediment grain size. Therefore, desiccated lacustrine sediments around the edge of the lake could act as a potential dust source for the CLP. This inference assumes that the northeastern Qaidam Plio-Quaternary samples (Pullen et al., 2011) have similar zircon U–Pb age distribution patterns to those deposited ~8 Ma. This assumption is reasonable considering that the sediments in northeastern Qaidam have been mainly derived from northeastern sources since at least the mid-late Miocene (Yin et al., 2008; Zhuang et al., 2011). Second, Zhuang et al. (2011) reveal that alluvial fans developed widely in northern Qaidam around 8 Ma. Derbyshire et al. (1998) proposed that silts deflated from surfaces of alluvial fans could be a major contribution to the loess accumulation on the CLP. Third, studies have demonstrated that the Asian continental interior experienced a short dry interval around 8 Ma, which might be genetically related to Tibetan plateau uplift around the same time (Jia et al., 2012; Rea et al., 1998). Therefore, part of the Qaidam Basin was possibly covered by sand seas around 8 Ma, from which CLP dust may have been stored or derived, similar to the situation hypothesized for modern deserts acting as dust sources for the CLP.

No matter which of these sources is dominant, materials would have to be transported to the CLP from Qaidam mainly via lower-level westerly winds and zircons from CN-8 Ma should be mainly of silt size. However, the mean zircon grain size of the CN-8 Ma sample (59×81 μm) is similar to that of the Liupan sample (62×85 μm), and significantly coarser than the three Red Clay samples above (Table 2 and Supplementary Fig. 10). Thus, despite the likely Qaidam origin, the hypothesis that the Liupan Mountains are a provenance region for the CLP at 8 Ma cannot be excluded (Guo et al., 2001). Previous work reported rapid exhumation of the Liupan Mountains around 8 Ma based on almost constant apatite fission track ages of 8 Ma (Zheng et al., 2006). Based on the high abundance of ages between 450 and 400 Ma for both CN-8 Ma and Liupan and the similar zircon grain size in the samples (Table 2, Fig. 6 and Supplementary Fig. 3), we argue that the 8 Ma sediments from Chaona will likely have some contribution from the rapidly exhumed Liupan Mountains. However, because Liupan also has more ages distributed between 300 and 200 Ma and 1000 and 700 Ma (Fig. 6), which is different for the CN-8 Ma sample, we infer that the Qaidam Basin must be another important prove-

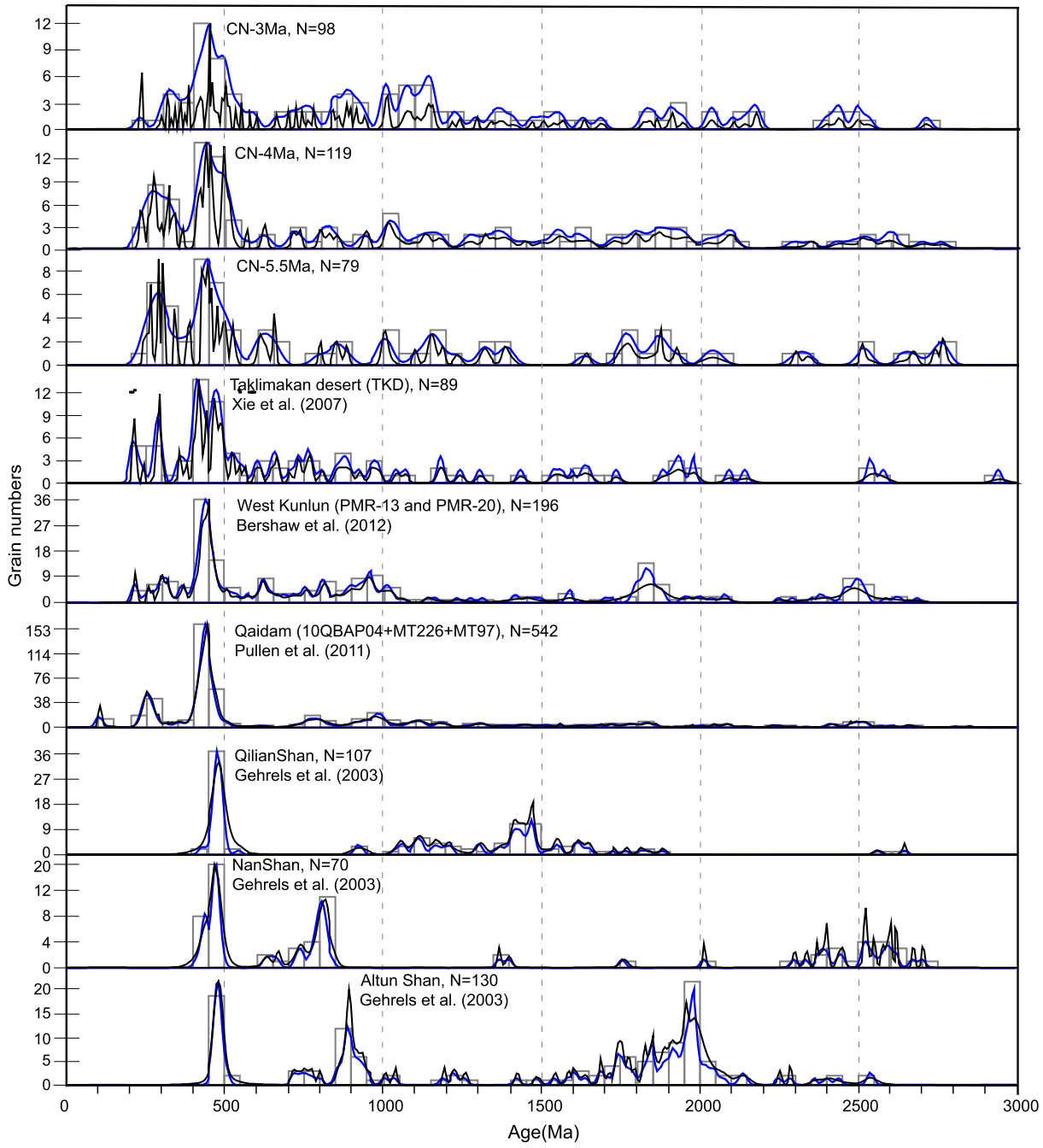

Fig. 7. A comparison of detrital zircon U–Pb ages between CN-5.5 Ma, CN-4 Ma, CN-3 Ma Red Clay samples and CLP distal source regions. Black and blue lines are normalized probability density function (PDF) and Kernel Density Estimation (KDE) plots, respectively, and the open rectangles are age histograms. (For interpretation of the references to color in this figure legend, the reader is referred to the web version of this article.)

nance for the CLP at 8 Ma. Furthermore, the peak zircon U–Pb age at 440 Ma for CN-8 Ma is closer to those of samples from the Qaidam basin, but not with Liupan (Fig. 6 and Supplementary Fig. 3). Thus, eolian deposition over this part of the CLP was initiated at least by late Miocene times. We therefore infer that the onset of Red Clay accumulation on the central CLP is a direct result of late Miocene uplift of the Liupan Mountains and the northeastern Tibetan Plateau (Fang et al., 2007, 2005; Hough et al., 2011; Lease et al., 2007; Zheng et al., 2006), which not only ended subsidence in the Longzhong Basin and produced a higher base elevation for eolian sediments to accumulate (Horton et al., 2004; Song et al., 2001; Wang et al., 2012), but also provided dusts to the CLP associated with the resultant Asian drying, lake shrinking, high altitude weathering, and alluvial fan formation in the Qaidam Basin (Fig. 9).

Table 2
Zircon grain size statistics from the Chaona Red Clay sequence and the Liupan sample. STD: standard deviation.

	CN-3 Ma	CN-4 Ma	CN-5.5 Ma	CN-8 Ma	Liupan
Length (um)	56	55	51	81	85
STD_Length	12	15	13	22	20
Width (um)	47	44	37	59	62
STD_Width	10	10	9	15	14

Our zircon U–Pb MDS analysis reveals that CN-5.5 Ma and CN-4 Ma Red Clay samples have detrital zircon spectra similar to those of the Taklamakan Desert, as well as from the

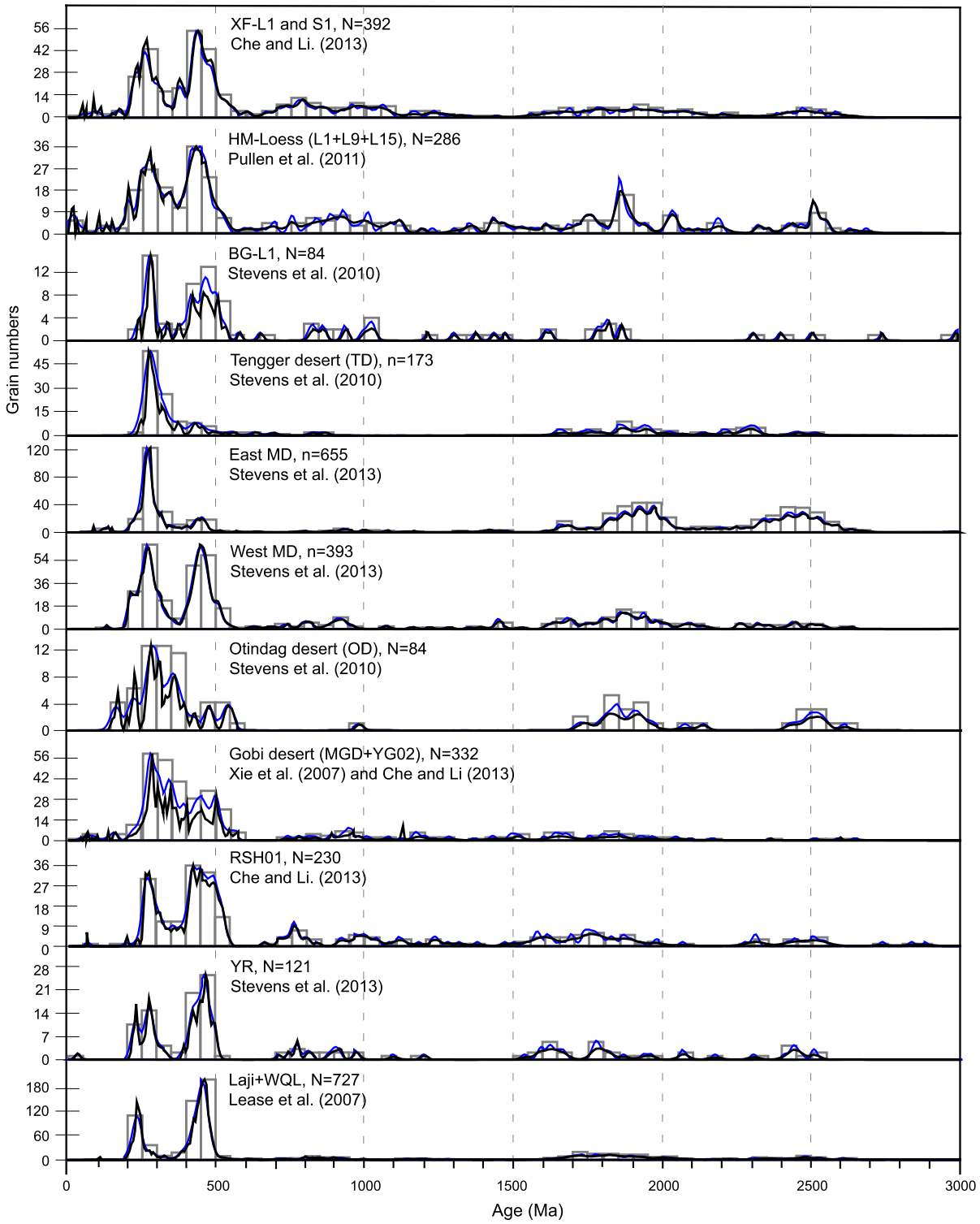

Fig. 8. A comparison of detrital zircon U–Pb ages between Quaternary loess and paleosol samples and CLP proximal deserts and river samples. Black and blue lines are normalized probability density function (PDF) and Kernel Density Estimation (KDE) plots, respectively, and the open rectangles are age histograms. (For interpretation of the references to color in this figure legend, the reader is referred to the web version of this article.)

western Kunlun terrane and Pamir on the northwestern Tibetan plateau, likely sources of the Taklamakan Desert sediment. Interestingly, Sun and Liu (2006) found that the age of the Taklamakan Desert is ~5.3 Ma, matching approximately the ages of these samples. In addition, the mean zircon grain size for CN-5.5 Ma is 37 × 51 μm, significantly finer than CN-3 Ma and CN-8 Ma (Table 2 and Supplementary Fig. 10), supporting a more distal CLP provenance. This is consistent with the bulk grain size trend shown from the CLP for the late Cenozoic (Sun et al., 2006). Therefore, we infer that dust was transported to the CLP mainly from the Taklamakan Desert via lower-level westerly winds for the time interval ~5.5–4 Ma (Fig. 9). As such, this transition to Taklamakan sources suggests dust generation and transport to the CLP linked to Asian aridification during the early Pliocene. In accordance with Sun and Liu (2006), we argue that both Tibetan plateau uplift and the Mediter-

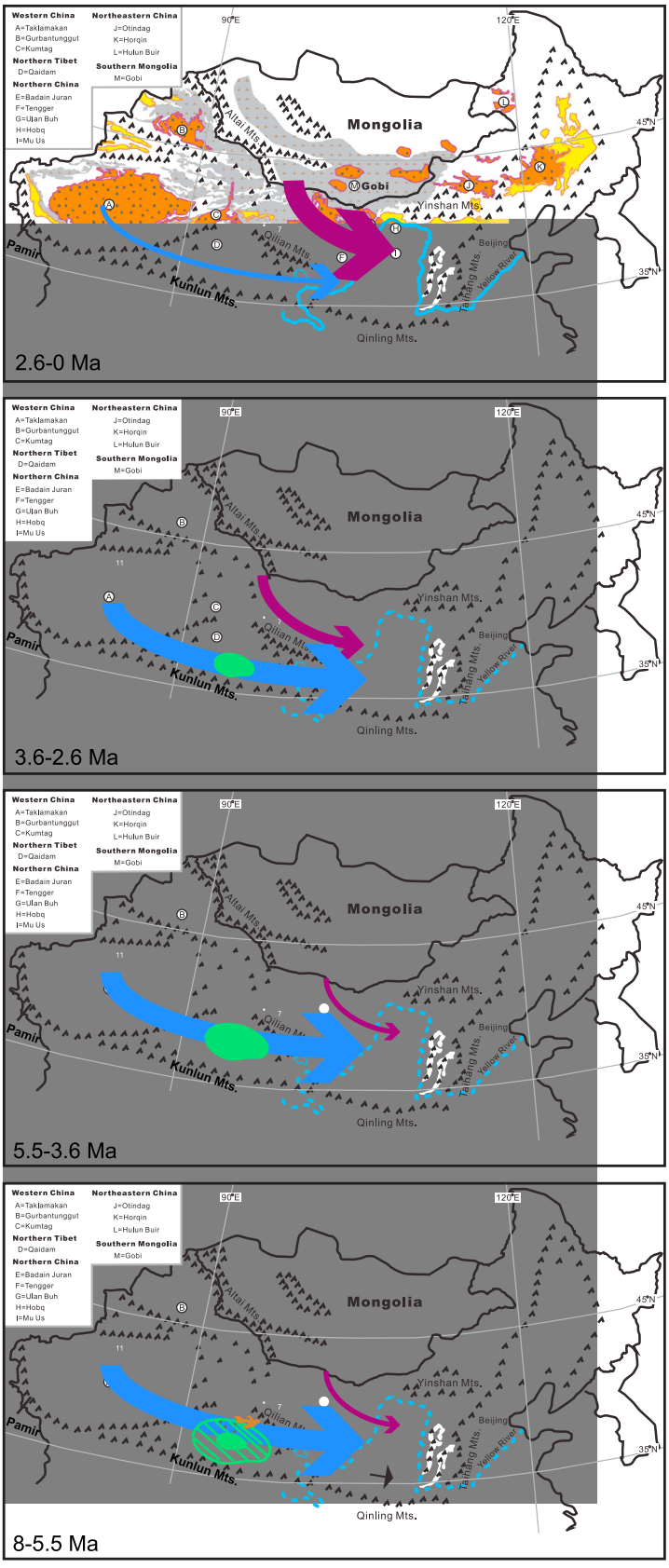

Fig. 9. Schematic dust transport routes for the 8–5.5 Ma, 5.5–3.6 Ma, 3.6–2.6 Ma, and the Quaternary. The width of arrow represents the relative importance of monsoon versus westerly wind induced dust transportation to the CLP. The green oval area indicates the schematic area of lacustrine sediments within the Qaidam Basin, which could serve as dust source materials during low lake levels. The hatched green area in the bottom panel represents exposed lacustrine sediment during central Asian drying (Rea et al., 1998) and lowered lake level (Fang et al., 2007) in the Qaidam Basin around 8 Ma. The black arrow in the bottom panel indicates that the Liupan Mountains also contribute zircons at that time to the CLP. The legend is the same as in Fig. 1. Dashed blue line in the bottom three subfigures indicates that uncertainty over whether the Yellow River had formed at these time periods. (For interpretation of the references to color in this figure legend, the reader is referred to the web version of this article.)

ranean salinity crisis would decrease moisture supply to inland Asia and cause the formation of the Taklamakan Desert at that time.

The CN-3 Ma Red Clay sample from the late Pliocene shows a decreased contribution from 300–200 Ma age grains (Fig. 3). We attribute this to dilution of the detrital contribution from the Taklamakan Desert with more materials originating further east from the northern Tibetan plateau and adjacent deserts, likely the Qilian Mountains and/or the Qaidam Basin (Fig. 9). This inference is consistent with pollen and dust accumulation evidence, suggesting an expanded desert dust source region driven by increased aridity after 3.6 Ma, associated with initiation of the Northern Hemisphere glaciations (Rea et al., 1998; Wu et al., 2011). A strong uplift phase of the Tibetan Plateau has been proposed to occur during 3.6–2.6 Ma (Fang et al., 2005; Li et al., 1997), which has the potential to be a strong candidate for driving this late Pliocene onset of the Northern Hemisphere glaciations (Mudelsee and Raymo, 2005) and potentially further causing dust source activation. However, the evidence used to infer late Pliocene uplift of the Tibetan Plateau is controversial (Nie et al., 2008b; Zhang et al., 2001). Therefore, whether the initiation of the Northern Hemisphere glaciations and/or expansion of aridity is a direct result of late Pliocene Tibetan uplift continues to be an open question (Nie et al., 2014; Raymo, 1994).

A comparison of CLP western and northern deserts reveals that the CLP northern deserts have a more pronounced component of 300–200 Ma zircon U–Pb ages, while the western deserts have more 500–400 Ma ages (Fig. 2). Thus, the increased 300–200 Ma age components for Quaternary loess samples suggests that more dust is being generated from the CLP northern deserts during the Quaternary, or directly from their likely source regions in northeastern Tibetan plateau and the Gobi Altai (Che and Li, 2013; Stevens et al., 2013b). This indicates a stronger winter monsoon and the development of the CLP northern deserts during the Quaternary (Fig. 9). Materials eroded from the Laji and the West Qinling Mountains, immediately south and west of the CLP, can also potentially contribute dust to the CLP for loess samples. However, considering that East Asian winter monsoon dominated the CLP during glacial periods of the Quaternary (Fig. 1) its contribution was probably smaller than that of sources north or northwest of the CLP. The onset of the intensive Northern Hemisphere glaciations after 2.7 Ma would have enhanced the Siberian High pressure system and intensified winter monsoon circulation, with associated increases in aridity (Ding et al., 2000; Sun, 2002).

These conclusions suggest that there has been a progressive eastward expansion of deserts since the Pliocene in Asia. However, the shift of Quaternary dust source signatures to those of the CLP proximal deserts may not imply expansion of these deserts right at the onset of the Quaternary. Indeed, drilling of sediments in the CLP proximal deserts reveals the deserts likely formed only during the middle Quaternary (Li et al., 2013b). Furthermore, uplift and/or drainage of high mountain areas such as the Gobi Altai and northeastern Tibetan plateau may play a major role in the transport of sediment to these desert sand sea areas, and potentially to the CLP (Stevens et al., 2013b; Yang et al., 2011), irrespective of aridity shifts. Thus, while the overall pattern of source shifts suggests a progressive eastward aridification during the Pliocene–Quaternary, further work is needed to clarify both the role of northern deserts versus alluvial fans in front of high mountain areas or fluvial sediments as direct sources for the Quaternary loess and the exact timing of CLP northern deserts' formation.

One issue with comparing sources through time on the CLP is that the Miocene–Pliocene Red Clay is finer grained than Quaternary loess (Sun et al., 2006), and laser spot sizes used in this study might bias the age results of Red Clay toward more CLP northern proximal sources. This may imply that our results show a selective bias to more locally derived zircons in the Red Clay sequence in comparison to Quaternary loess. However, we suggest this would only be a minor effect because zircon age distributions here demonstrate more CLP northern proximal sources for Quaternary loess. As such, this observation suggests that considering grain size variations strengthens our conclusions about the eastward expansion of the Asian deserts. The CN-8 Ma is an exception to this argument. Zircons in CN-8 Ma and Liupan are coarser than the overlying Pliocene Red Clay and Quaternary loess and as such we used 32 μm laser spot size to ablate most zircon grains. If the CN-8 Ma is entirely sourced from the Liupan Mountains, CN-8 Ma and Liupan should have similar age distribution patterns. In contrast, we observed that CN-8 Ma is more similar to Qaidam samples, suggesting that the Qaidam Basin likely contributed materials to the CLP around 8 Ma and the bottom Red Clay sequence contains sediment derived from both the Liupan Mountains and the Qaidam Basin, governed more by uplift than aridification.

This study is the first zircon U–Pb geochronology data for the Red Clay sequence on the CLP and we suggest that the findings are likely representative of the Red Clay in general, due to its far traveled eolian origin. However, Wang et al. (2012) reported rather dissimilar zircon U–Pb data from coeval fluvial and alluvial strata in the nearby Ningxia Basin. This is likely to be an artifact of the nature of the samples studied in Wang et al. (2012); coarse to medium-grained sandstones that are clearly locally derived from surrounding mountains and the Alaxa block, transported through fluvial or alluvial processes. Accordingly, they used a larger laser spot size of 40–65 μm (Wang et al., 2012) than our study, which will make their results more biased to local sources. In contrast, our Red Clay samples are silt-sized and have a significant far traveled eolian contribution. Thus, although clear differences in zircon U–Pb age distribution patterns exist between the samples of Wang et al. (2012) and the coeval Red Clay samples here, this difference does not help to constrain whether the provenance of the Red Clay is spatially variable. Clearly, more zircon U–Pb geochronology work needs to be performed to more Red Clay sections to fully answer this question.

5. Conclusions

1. The late Miocene lowermost Red Clay is sourced from both the Qaidam Basin and the Liupan Mountains, transported via the lower-level westerly winds and fluvial systems, respectively.

2. The early–mid Pliocene Red Clay deposited during 5.5–4 Ma has a western Kunlun/Pamir provenance, suggesting that the CLP distal Taklamakan Desert was the principal source and that dust material was transported to the CLP mainly via the lower-level westerly winds.

3. The upper Red Clay of the late Pliocene is sourced from multiple areas, likely including northern Tibetan plateau, Taklimakan and Qaidam Desert sediments, and materials eroded from the Qilian Mountains.

4. In comparison to the Pliocene Red Clay, Quaternary loess sediments have more contribution from CLP proximal deserts and the Yellow River, which in turn may be sourced from the Gobi Altai and northeastern Tibetan plateau.

5. These results demonstrate that Asian desertification has a pattern of eastward expansion since the late Miocene. The ages of expansions of Asian desertification are synchronous to both proposed phases of Tibetan uplift and global climatic changes, suggesting that Asian desertification was forced by both. However, evidence for uplift in the late Pliocene–Quaternary is controversial, implying that climatic controls may be key to activation of dust sources of this time period.

Acknowledgements

We thank Z. Zhang and L. Stockli for help with dating zircons and F. Chen and X. Zhang for useful discussion about the westerly term. This paper benefited significantly from constructive suggestions from two reviewers and the Editor T. Harrison. This work is co-supported by the (973) National Basic Research Program of China (Grant No. 2013CB956400), the Strategic Priority Research Program of the Chinese Academy of Sciences (Grant No. XDB03020400), the National Natural Science Foundation of China (Grant Nos. 41172329; 41372036; 41321061; 41021091; 41290253), the Research Fund for the Doctoral Program of Higher Education of China (Grant No. 20110211110012), Scientific and Technological Innovation Team of Chinese Academy of Sciences, Natural Science Basis Research Plan in Shaanxi Province of China (2012JM5002), and China Postdoctoral Science Foundation (20100470538). T. Stevens and A. Bird gratefully acknowledge the support of Natural Environment Research Council (NERC) standard grant NE/I008837/1.

Appendix A. Supplementary material

Supplementary material related to this article can be found online at http://dx.doi.org/10.1016/j.epsl.2014.09.026.

References

An, Z., 2000. The history and variability of the East Asian paleomonsoon climate. Quat. Sci. Rev. 19, 171–187.

An, Z.S., Kutzbach, J.E., Prell, W.L., Porter, S.C., 2001. Evolution of Asian monsoons and phased uplift of the Himalaya–Tibetan plateau since Late Miocene times. Nature 411, 62–66.

Andersson, J.G., 1923. Essays on the Cenozoic of Northern China. Geol. Surv. China. Mem., Ser. A. 3, 107–114.

Bershaw, J., Garzione, C.N., Schoenbohm, L., Gehrels, G., Tao, L., 2012. Cenozoic evolution of the Pamir plateau based on stratigraphy, zircon provenance, and stable isotopes of foreland basin sediments at Oytag (Wuyitake) in the Tarim Basin (west China). J. Asian Earth Sci. 44, 136–148.

Chang, Z.S., Vervoort, J.D., McClelland, W.C., Knaack, C., 2006. U–Pb dating of zircon by LA-ICP-MS. Geochem. Geophys. Geosyst. 7, Q05009. http://dx.doi.org/10.1029/2005GC001100.

Chang, M.M., Wang, X.M., Liu, H.Z., Miao, D.S., Zhao, Q.H., Wu, G.X., Liu, J., Li, Q., Sun, Z.C., Wang, N., 2008. Extraordinarily thick-boned fish linked to the aridification of the Qaidam Basin (northern Tibetan Plateau). Proc. Natl. Acad. Sci. USA 105, 13246–13251.

Che, X., Li, G., 2013. Binary sources of loess on the Chinese Loess Plateau revealed by U–Pb ages of zircon. Quat. Res. 80, 545–551.

Chen, Z., Li, G., 2013. Evolving sources of eolian detritus on the Chinese Loess Plateau since early Miocene: tectonic and climatic controls. Earth Planet. Sci. Lett. 371–372, 220–225.

Chen, J., Li, G.J., Yang, J.D., Rao, W.B., Lu, H.Y., Balsam, W., Sun, Y.B., Ji, J.F., 2007. Nd and Sr isotopic characteristics of Chinese deserts: implications for the provenances of Asian dust. Geochim. Cosmochim. Acta 71, 3904–3914.

deMenocal, P.B., Rind, D., 1993. Sensitivity of Asian and African climate to variations in seasonal insolation, glacial ice cover, sea surface temperature, and Asian orography. J. Geophys. Res. 98, 7265–7287.

Derbyshire, E., Meng, X., Kemp, R.A., 1998. Provenance, transport and characteristics of modern aeolian dust in western Gansu Province, China, and interpretation of the Quaternary loess record. J. Arid Environ. 39, 497–516.

Dickinson, W.R., Gehrels, G.E., 2008. Sediment delivery to the Cordilleran foreland basin: insights from U–Pb ages of detrital zircons in upper Jurassic and Cretaceous strata of the Colorado Plateau. Am. J. Sci. 308, 1041–1082.

Ding, Z.L., Sun, J.M., Liu, T.S., Zhu, R.X., Yang, S.L., Guo, B., 1998. Wind-blown origin of the Pliocene red clay formation in the central Loess Plateau, China. Earth Planet. Sci. Lett. 161, 135–143.

Ding, Z.L., Xiong, S.F., Sun, J.M., Yang, S.L., Gu, Z.Y., Liu, T.S., 1999. Pedostratigraphy and paleomagnetism of a ~7.0 Ma eolian loess-red clay sequence at Lingtai, Loess Plateau, north-central China and the implications for paleomonsoon evolution. Palaeogeogr. Palaeoclimatol. Palaeoecol. 152, 49–66.

Ding, Z.L., Rutter, N.W., Sun, J.M., Yang, S.L., Liu, T.S., 2000. Re-arrangement of atmospheric circulation at about 2.6 Ma over northern China: evidence from grain size records of loess-paleosol and red clay sequences. Quat. Sci. Rev. 19, 547–558.

Ding, Z.L., Sun, J.M., Yang, S.L., Liu, T.S., 2001. Geochemistry of the Pliocene red clay formation in the Chinese Loess Plateau and implications for its origin, source provenance and paleoclimate change. Geochim. Cosmochim. Acta 65, 901–913.

Fang, X., Li, J.J., Van der Voo, R., 1999. Rock magnetic and grain size evidence for intensified Asian atmospheric circulation since 800,000 years B.P. related to Tibetan uplift. Earth Planet. Sci. Lett. 165, 129–144.

Fang, X.M., Yan, M., Van der Voo, R., Rea, R., Song, C., Pares, J., Gao, G., Nie, J., Dai, S., 2005. Late Cenozoic deformation and uplift of the NE Tibetan Plateau: evidence from high-resolution magnetostratigraphy of the Guide Basin, Qinghai Province, China. Geol. Soc. Am. Bull. 117, 1208–1225.

Fang, X., Zhang, W., Meng, Q., Gao, J., Wang, X., King, J., Song, C., Dai, S., Miao, Y., 2007. High resolution magnetostratigraphy of the Neogene Huaitoutala section in the eastern Qaidam Basin on the NE Tibetan Plateau, Qinghai Province, China and its implication on tectonic uplift of the NE Tibetan Plateau. Earth Planet. Sci. Lett. 258, 293–306.

Fu, C., An, Z., 2002. Study of aridification in northern China—a global change issue facing directly the demand of nation. Earth Sci. Front. 9, 271–275.

Gallet, S., Jahn, B.M., Torii, M., 1996. Geochemical characterization of the Luochuan loess-paleosol sequence, China, and paleoclimatic implications. Chem. Geol. 133, 67–88.

Gehrels, G.E., Yin, A., Wang, X.F., 2003. Detrital-zircon geochronology of the northeastern Tibetan plateau. Geol. Soc. Am. Bull. 115, 881–896.

Gehrels, G., Kapp, P., DeCelles, P., Pullen, A., Blakey, R., Weislogel, A., Ding, L., Guynn, J., Martin, A., McQuarrie, N., Yin, A., 2011. Detrital zircon geochronology of pre-Tertiary strata in the Tibetan–Himalayan orogen. Tectonics 30, TC5016.

Guan, Q.Y., Pan, B.T., Gao, H.S., Li, N., Zhang, H., Wang, J.P., 2008. Geochemical evidence of the Chinese loess provenance during the Late Pleistocene. Palaeogeogr. Palaeoclimatol. Palaeoecol. 270, 53–58.

Guo, Z.T., Peng, S.Z., Hao, Q.Z., Biscaye, P.E., Liu, T.S., 2001. Origin of the Miocene–Pliocene red-earth formation at Xifeng in Northern China and implications for paleoenvironments. Palaeogeogr. Palaeoclimatol. Palaeoecol. 170, 11–26.

Guo, Z.T., Ruddiman, W.F., Hao, Q.Z., Wu, H.B., Qiao, Y.S., Zhu, R.X., Peng, S.Z., Wei, J.J., Yuan, B.Y., Liu, T.S., 2002. Onset of Asian desertification by 22 Myr ago inferred from loess deposits in China. Nature 416, 159–163.

Heermance, R.V., Pullen, A., Kapp, P., Garzione, C.N., Bogue, S., Ding, L., Song, P., 2013. Climatic and tectonic controls on sedimentation and erosion during the Pliocene–Quaternary in the Qaidam Basin (China). Geol. Soc. Am. Bull. 125, 833–856.

Horton, B.K., Dupont-Nivet, G., Zhou, J., Waanders, G.L., Butler, R.F., Wang, J., 2004. Mesozoic–Cenozoic evolution of the Xining-Minhe and Dangchang basins, northeastern Tibetan Plateau: magnetostratigraphic and biostratigraphic results. J. Geophys. Res. 109, B04402. http://dx.doi.org/10.1029/2003JB002913.

Hough, B.G., Garzione, C.N., Wang, Z., Lease, R.O., Burbank, D.W., Yuan, D., 2011. Stable isotope evidence for topographic growth and basin segmentation: implications for the evolution of the NE Tibetan Plateau. Geol. Soc. Am. Bull. 123, 168–185.

Jackson, S.E., Pearson, N.J., Griffin, W.L., Belousova, E.A., 2004. The application of laser ablation-inductively coupled plasma-mass spectrometry to in situ U–Pb zircon geochronology. Chem. Geol. 211, 47–69.

Jia, G., Li, Z., Peng, P.a., Zhou, L., 2012. Aeolian *n*-alkane isotopic evidence from North Pacific for a Late Miocene decline of C_4 plant in the arid Asian interior. Earth Planet. Sci. Lett. 321–322, 32–40.

Kapp, P., Pelletier, J.D., Rohrmann, A., Heermance, R., Russell, J., Ding, L., 2011. Wind erosion in the Qaidam basin, central Asia: implications for tectonics, paleoclimate, and the source of the Loess Plateau. GSA Today 21, 4–10.

Lease, R.O., Burbank, D.W., Gehrels, G.E., Wang, Z.C., Yuan, D.Y., 2007. Signatures of mountain building: detrital zircon U/Pb ages from northeastern Tibet. Geology 35, 239–242.

Li, J.J., 1995. Uplift of Qingha-Xizang Plateau and Global Change. Lanzhou University Press, Lanzhou, pp. 181–207.

Li, J.J., Fang, X.M., Van der Voo, R., Zhu, J.J., Mac Niocaill, C., Cao, J.X., Zhong, W., Chen, H.L., Wang, J.L., Wang, J.M., Zhang, Y.C., 1997. Late Cenozoic magnetostratigraphy (11–0 Ma) of the Dongshanding and Wangjiashan section in the Longzhong Basin, western China. Geol. Mijnb. 76, 121–134.

Li, X., Dong, G., Jin, H., Su, Z., Wang, Y., 1999. Discovery of Ordos Cretaceous dune rock and its significance. Chin. Sci. Bull. 44, 2102–2106.

Li, M.H., Fang, X.M., Wang, J.Y., Song, Y.G., Yang, Y.B., Zhang, W.L., Liu, X.M., 2013a. Evaporite minerals of the lower 538.5 m sediments in a long core from the Western Qaidam Basin, Tibet. Quat. Int. 298, 123–133.

Li, Z., Sun, D., Chen, F., Wang, F., Zhang, Y., Guo, F., Wang, X., Li, B., 2013b. Chronology studies of a drill core in the central Tengger Desert of China and its implication for Asian desertification. Quat. Sci. Rev. 85, 85–98.

Liu, T.S., 1985. Loess and the Environment. China Ocean, Beijing.

Liu, X., Xu, T., Liu, T., 1988. The Chinese loess in Xifeng, II. A study of anisotropy of magnetic susceptibility of loess from Xifeng. Geophys. J. 92, 349–353.

Liu, X., Rolph, T.C., An, Z.S., Hesse, P., 2003. Paleoclimatic significance of magnetic properties on the Red Clay underlying the loess and paleosols in China. Palaeogeogr. Palaeoclimatol. Palaeoecol. 199, 153–166.

Lu, H., An, Z., 1998. Paleoclimatic significance of grain size of loess-palaeosol deposit in Chinese Loess Plateau. Sci. China, Ser. D 41, 626–631.

Lu, H.Y., Vandenberghe, J., An, Z.S., 2001. Aeolian origin and palaeoclimatic implications of the 'Red Clay' (north China) as evidenced by grain-size distribution. J. Quat. Sci. 16, 89–97.

Lu, H.Y., Mason, J.A., Stevens, T., Zhou, Y.L., Yi, S.W., Miao, X.D., 2011. Response of surface processes to climatic change in the dunefields and Loess Plateau of North China during the late Quaternary. Earth Surf. Process. Landf. 36, 1590–1603.

Ludwig, K.R., 2003. User's Manual for Isoplot 3.00 a Geochronological Toolkit for Microsoft Excel.

Maher, B.A., Mutch, T.J., Cunningham, D., 2009. Magnetic and geochemical characteristics of Gobi Desert surface sediments: implications for provenance of the Chinese Loess Plateau. Geology 37, 279–282.

Miao, X., Sun, Y., Lu, H., Mason, J.A., 2004. Spatial pattern of grain size in the Late Pliocene 'Red Clay' deposits (North China) indicates transport by low-level northerly winds. Palaeogeogr. Palaeoclimatol. Palaeoecol. 206, 149–155.

Miao, Y.F., Herrmann, M., Wu, F.L., Yan, X.L., Yang, S.L., 2012. What controlled Mid-Late Miocene long-term aridification in Central Asia? Global cooling or Tibetan Plateau uplift: a review. Earth-Sci. Rev. 112, 155–172.

Mudelsee, M., Raymo, M.E., 2005. Slow dynamics of the Northern Hemisphere glaciation. Paleoceanography 20, PA4022. http://dx.doi.org/10.1029/2005PA001153.

Nie, J., Peng, W., 2014. Automated SEM–EDS heavy mineral analysis reveals no provenance shift between glacial loess and interglacial paleosol on the Chinese Loess Plateau. Aeolian Res. 13, 71–75.

Nie, J., King, J., Fang, X., 2007. Enhancement mechanisms of magnetic susceptibility in the Chinese Red-Clay sequence. Geophys. Res. Lett. 34, L19705. http://dx.doi.org/10.1029/2007GL031430.

Nie, J., King, J.W., Fang, X., 2008b. Tibetan uplift intensified the 400 k.y. signal in paleoclimate records at 4 Ma. Geol. Soc. Am. Bull. 120, 1338–1344.

Nie, J., King, J., Jackson, M., Fang, X., Song, Y., 2008a. AC magnetic susceptibility studies of the Chinese red-clay sediments between 4.8–4.1 Ma and their paleoceanographic and paleoclimatic implications. J. Geophys. Res. 113, B10106. http://dx.doi.org/10.1029/2008JB005654.

Nie, J., Horton, B.K., Mora, A., Saylor, J.E., Housh, T.B., Rubiano, J., Naranjo, J., 2010. Tracking exhumation of Andean ranges bounding the Middle Magdalena Valley Basin, Colombia. Geology 38, 451–454.

Nie, J., Peng, W., Pfaff, K., Möller, A., Garzanti, E., Andò, S., Stevens, T., Bird, A., Chang, H., Song, Y., Liu, S., Ji, S., 2013. Controlling factors on heavy mineral assemblages in Chinese loess and Red Clay. Palaeogeogr. Palaeoclimatol. Palaeoecol. 381–382, 110–118.

Nie, J., Stevens, T., Song, Y., King, J., Zhang, R., Ji, S., Gong, L., Cares, D., 2014. Pacific freshening drives Pliocene cooling and Asian monsoon intensification. Sci. Rep. 4, 5474. http://dx.doi.org/10.1038/srep05474.

Paton, C., Hellstrom, J., Paul, B., Woodhead, J., Hergt, J., 2011. Iolite: freeware for the visualisation and processing of mass spectrometric data. J. Anal. At. Spectrom. http://dx.doi.org/10.1039/C1JA10172B.

Pullen, A., Kapp, P., McCallister, A.T., Chang, H., Gehrels, G.E., Garzione, C.N., Heermance, R.V., Ding, L., 2011. Qaidam Basin and northern Tibetan Plateau as dust sources for the Chinese Loess Plateau and paleoclimatic implications. Geology 39, 1031–1034.

Ramstein, G., Fluteau, F., Besse, J., Joussaume, S., 1997. Effect of orogeny, plate motion and land–sea distribution on Eurasian climate change over the past 30 million years. Nature 386, 788–795.

Raymo, M.E., 1994. The initiation of Northern Hemisphere glaciation. Annu. Rev. Earth Planet. Sci. 22, 353–383.

Rea, D.K., Snoeckx, H., Joseph, L.H., 1998. Late Cenozoic eolian deposition in the North Pacific: Asian drying, Tibetan uplift, and cooling of the northern hemisphere. Paleoceanography 13, 215–224.

Riggs, N.R., Lehman, T.M., Gehrels, G.E., Dickinson, W.R., 1996. Detrital zircon link between headwaters and terminus of the upper Triassic Chinle-Dockum paleoriver system. Science 273, 97–100.

Ruddiman, W.F., Raymo, M.E., 1988. Northern hemisphere climate regimes during the past 3 Ma: possible tectonic connections. In: Shackleton, N.J., West, R.G., Bowen, D.Q. (Eds.), The Past Three Million Years: Evolution of Climatic Variability in the North Atlantic Region. Cambridge University Press, Cambridge, pp. 227–234.

Sláma, J., Košler, J., Condon, D.J., Crowley, J.L., Gerdes, A., Hanchar, J.M., Horstwood, M.S.A., Morris, G.A., Nasdala, L., Norberg, N., Schaltegger, U., Schoene, B., Tubrett, M.N., Whitehouse, M.J., 2008. Plešovice zircon — a new natural reference material for U–Pb and Hf isotopic microanalysis. Chem. Geol. 249, 1–35.

Smalley, I.J., Kumar, R., Dhand, K.O., Jefferson, I.F., Evans, R.D., 2005. The formation of silt material for terrestrial sediments: particularly loess and dust. Sediment. Geol. 179, 321–328.

Song, Y., Fang, X., Li, J.J., An, Z.S., Miao, X., 2001. The Late Cenozoic uplift of the Liupan Shan, China. Sci. China, Ser. D supp. 44, 176–184.

Stevens, T., Palk, C., Carter, A., Lu, H., Clift, P.D., 2010. Assessing the provenance of loess and desert sediments in northern China using U–Pb dating and morphology of detrital zircons. Geol. Soc. Am. Bull. 122, 1331–1344.

Stevens, T., Adamiec, G., Bird, A.F., Lu, H., 2013a. An abrupt shift in dust source on the Chinese Loess Plateau revealed through high sampling resolution OSL dating. Quat. Sci. Rev. 82, 121–132.

Stevens, T., Carter, A., Watson, T.P., Vermeesch, P., Lu, H., Ando, S., Garzanti, E., Bird, A.F., Cottam, M.A., Sevastjanova, I., 2013b. Genetic linkage between the Yellow River, the Mu Us desert, and the Chinese Loess Plateau. Quat. Sci. Rev. 78, 355–368.

Sun, J., 2002. Provenance of loess material and formation of loess deposits on the Chinese Loess Plateau. Earth Planet. Sci. Lett. 203, 845–859.

Sun, J., Liu, T., 2006. The age of the Taklimakan desert. Science 312, 1621.

Sun, D., Liu, T., Chen, M., An, Z., 1997. Magnetostratigraphy and palaeoclimate of Red Clay sequences from Chinese loess Plateau. Sci. China, Ser. D 40, 337–343.

Sun, J., Zhang, M., Liu, T., 2001. Spatial and temporal characteristics of dust storms in China and its surrounding regions, 1960–1999: relations to source area and climate. J. Geophys. Res. 106, 10325–10333.

Sun, Y., Lu, H.Y., An, Z.S., 2006. Grain size of loess, palaeosol and Red Clay deposits on the Chinese Loess Plateau: significance for understanding pedogenic alteration and palaeomonsoon evolution. Palaeogeogr. Palaeoclimatol. Palaeoecol. 241, 129–138.

Sun, Y.B., Tada, R.J., Chen, J.C., Liu, Q.S., Toyoda, S., Tani, A., Ji, J.F., Isozaki, Y., 2008. Tracing the provenance of fine-grained dust deposited on the central Chinese Loess Plateau. Geophys. Res. Lett. 35, L01804. http://dx.doi.org/10.1029/2007GL031672.

Sun, J.M., Ye, J., Wu, W.Y., Ni, X.J., Bi, S.D., Zhang, Z.Q., Liu, W.M., Meng, J., 2010. Late Oligocene–Miocene mid-latitude aridification and wind patterns in the Asian interior. Geology 38, 515–518.

Vermeesch, P., 2012. On the visualisation of detrital age distributions. Chem. Geol. 312, 190–194.

Vermeesch, P., 2013. Multi-sample comparison of detrital age distributions. Chem. Geol. 341, 140–146.

Wang, W., Kirby, E., Peizhen, Z., Dewen, Z., Guangliang, Z., Huiping, Z., Wenjun, Z., Chizhang, C., 2012. Tertiary basin evolution along the northeastern margin of the Tibetan Plateau: evidence for basin formation during Oligocene transtension. Geol. Soc. Am. Bull. 125, 377–400.

Watson, A.J., Bakker, D.C.E., Ridgwell, A.J., Boyd, P.W., Law, C.S., 2000. Effect of iron supply on Southern Ocean CO_2 uptake and implications for glacial atmospheric CO_2. Nature 407, 730–733.

Weislogel, A.L., Graham, S.A., Chang, E.Z., Wooden, J.L., Gehrels, G.E., Yang, H.S., 2006. Detrital zircon provenance of the Late Triassic Songpan–Ganzi complex: sedimentary record of collision of the North and South China blocks. Geology 34, 97–100.

Wu, F.L., Fang, X.M., Herrmann, M., Mosbrugger, V., Miao, Y.F., 2011. Extended drought in the interior of Central Asia since the Pliocene reconstructed from sporopollen records. Glob. Planet. Change 76, 16–21.

Xiao, G., Zong, K., Li, G., Hu, Z., Dupont-Nivet, G., Peng, S., Zhang, K., 2012. Spatial and glacial–interglacial variations in provenance of the Chinese Loess Plateau. Geophys. Res. Lett. 39, L20715. http://dx.doi.org/10.1029/2012GL053304.

Xie, J., Wu, F.Y., Ding, Z.L., 2007. Detrital zircon composition of U–Pb ages and Hf isotope of the Hunshandake sandland and implications for its provenance. Acta Petrol. Sin. 23, 523–528.

Yang, X., Scuderi, L., Paillou, P., Liu, Z., Li, H., Ren, X., 2011. Quaternary environmental changes in the drylands of China—a critical review. Quat. Sci. Rev. 30, 3219–3233.

Yin, A., Harrison, T.M., 2000. Geologic evolution of the Himalayan–Tibetan orogen. Annu. Rev. Earth Planet. Sci. 28, 211–280.

Yin, A., Dang, Y.Q., Wang, L.C., Jiang, W.M., Zhou, S.P., Chen, X.H., Gehrels, G.E., McRivette, M.W., 2008. Cenozoic tectonic evolution of Qaidam basin and its surrounding regions (Part 1): the southern Qilian Shan–Nan Shan thrust belt and northern Qaidam basin. Geol. Soc. Am. Bull. 120, 813–846.

Zachos, J., Pagani, M., Sloan, L., Thomas, E., Billups, K., 2001. Trends, rhythms, and aberrations in global climate 65 Ma to present. Science 292, 686–693.

Zhang, P., Molnar, P., Downs, W.R., 2001. Increased sedimentation rates and grain sizes 2–4 Myr ago due to the influence of climate change on erosion rates. Nature 410, 891–897.

Zheng, D., Zhang, P.-Z., Wan, J., Yuan, D., Li, C., Yin, G., Zhang, G., Wang, Z., Min, W., Chen, J., 2006. Rapid exhumation at ~8 Ma on the Liupan Shan thrust fault from apatite fission-track thermochronology: implications for growth of the northeastern Tibetan Plateau margin. Earth Planet. Sci. Lett. 248, 198–208.

Zhuang, G., Hourigan, J.K., Ritts, B.D., Kent-Corson, M.L., 2011. Cenozoic multiple-phase tectonic evolution of the northern Tibetan Plateau: constraints from sedimentary records from Qaidam basin, Hexi Corridor, and Subei basin, northwest China. Am. J. Sci. 311, 116–152.